Plasmonics (2017) 12:1037–1043
DOI 10.1007/s11468-016-0356-5

Tunable Plasmonic Absorber Based on Propagating and Localized Surface Plasmons Using Metal-Dielectric-Metal Structure

Qiang Li[1,2] · Jinsong Gao[1,2] · Haigui Yang[1] · Hai Liu[1] · Xiaoyi Wang[1] · Zizheng Li[1,2] · Xin Guo[2,3]

Received: 22 June 2016 / Accepted: 8 August 2016 / Published online: 19 August 2016

Abstract We propose a metal-dielectric-metal super absorber based on propagating and localized surface plasmons which exhibits a near perfect absorption in the visible and near-infrared spectrum. The absorber consists of $Ag/Al_2O_3/Al$ triple layers in which the top Al layer is a periodic nano disk array. The absorption spectrum can be easily controlled by adjusting the structure parameters including the period and radius of the nano disk and the maximal absorption can reach 99.62 %. We completely analyze the PSPs and LSPs modes supported by the MDM structure and their relationship with the ultrahigh absorption. Moreover, we propose a novel idea to further enhance the absorption by exciting the PSPs and high-order LSPs modes simultaneously, which is different from the previous works. This kind of absorber using stable inexpensive Al instead of noble metal Au or Ag is an appropriate candidate for photovoltaics, spectroscopy, photodetectors, sensing, and surface-enhanced Raman spectroscopy (SERS).

Keywords Surface plasmons · Nanostructures · Plasmonics · Metal-dielectric-metal structure · Super absorber

✉ Haigui Yang
liqiang113@mails.ucas.ac.cn

[1] Key Laboratory of Optical System Advanced Manufacturing Technology, Changchun Institute of Optics, Fine Mechanics and Physics, Chinese Academy of Sciences, Changchun 130033, China

[2] University of the Chinese Academy of Sciences, Beijing 100039, China

[3] Shanghai Institute of Applied Physics, Chinese Academy of Science, Shanghai 201800, China

Introduction

Super absorber [1] has attracted much attention due to its greatly potential applications in solar cell [2, 3], photo detectors [4], sensing [5], and thermal emitting [6]. The first absorber was created in 1952 for the military to absorb radar waves with a three-layer structure, but it was eliminated for its bulk thickness [7]. Recently, surface plasmon resonance (SPR) around metallic nanostructures provides an unprecedented way to manipulate the interaction between the light and matter at nanoscale, which plays a vital role in various fields such as imaging [8], color filter [9], surface-enhanced Raman scattering (SERS) [10], and energy harvest [11]. The SPR is a collective oscillation of electrons at the interface of metal and dielectric. It can be categorized into propagating surface plasmons (PSPs) and localized surface plasmons (LSPs) [12]. Many absorbers based on plasmonic structures working from the microwave to the visible regime were proposed and exhibited an ultrahigh tunable absorption spectrum by engineering the shape, size, material of the structure as well as its dielectric environment [13–15].

The super absorbers based on surface plasmons in many previous works usually consist of a triple metal-dielectric-metal (MDM) layers, in which the top patterned nanostructure is usually the noble metals such as gold (Au) and silver (Ag) [16, 17]. However, Au is costly that turns out to be a challenge for the application in large area. What is worse, Au has intrinsic interband transition leading to a dissipative channel below the wavelength of 550 nm. While the plasmonic structure made of Ag is extremely easy to be vulcanized or oxidized. Most recently, Aluminum (Al) has attracted much attention for plasmonic structures because its d-band lies above its Fermi energy supporting tunable plasmon resonance in the entire visible spectrum [18, 19]. Compared to the noble metals, Al also has many advantages including stable quality, low cost, ease of processing, and large storage on the earth.

In this paper, we propose a triple metal-dielectric-metal structure which consists of a periodic nano Al disk array spaced by a thin Al_2O_3 layer from a continuous Ag film as shown in Fig. 1a. The top Al disk array is the electric resonator, the bottom Ag layer serves as an optical mirror to ensure no light can pass through, and the middle ultra-thin dielectric layer acts as a cavity. The use of this plasmonic structure can excite three different modes: every individual unit cell for localized surface plasmons (LSPs), the periodic nano Al disk array for propagating surface plasmons (PSPs), and also the interaction between them (hybrid mode). By adjusting the structure parameters including the period and radius of the nano disk, we tune the electromagnetic modes in the visible and near-infrared spectrum so that an ultrahigh absorption can be achieved.

Numerical Investigation and Discussion

A representative unit geometry is schematically shown in Fig. 1b. We choose silicon (Si) as substrate. And the t, d, and h represent the thickness of the bottom Ag layer, Al_2O_3 spacing layer, and top Al disks. The radius and period of top patterned nano Al disks are r and L, respectively, as shown in Fig. 1c. In this structure, Ag is used for its low material absorption and high reflection in the entire visible and near-infrared wavelength ranges. The thickness of bottom Ag layer t is set to be 100 nm which is several times larger than the skin depth so that the incident light transmission through the structure can be completely inhibited. Therefore, the absorption is $A = 1\text{-}R$ where R is the reflection. The incident light with a wavelength range from 400 to 2000 nm propagates along the negative z direction with the E field polarization in the x direction as shown in Fig. 1a. The configuration of incident light remains unchanged in this work.

We perform the 3D finite-difference time-domain (FDTD) simulation to investigate the optical characteristic of the proposed absorber, where the periodic boundary conditions are used for a unit cell in the x-y plane and perfectly matched layers (PML) are applied in the z axis. A discrete mesh with the size of $2 \times 2 \times 1$ nm^3 was used for the cylinder disks. The optical constants of Ag, Al_2O_3, and Al used in simulation are extracted from the data of Palik [20]. Firstly, we sweep the period L with fixing h = 36 nm, d = 24 nm, and r = 160 nm and plot the absorption as a function of L and the wavelength of the incident wave. It is evident from Fig. 2a that three different modes lead to three distinct absorption peaks marked as B1, B2, and B3, in which the location of B1 strongly depends on the unit period L and B2, B3 stay constant with varying L. In accordance to previous works [10, 21], the LSP properties of a metal nanostructure mainly depend on its shape, size, material as well as the dielectric environment; the PSPs resonance frequency is determined by the array period and the angle of incident light. So in our situation, we attribute B1 mode to the excitation of PSPs by grating coupling, while B2, B3 modes are the LSPs around the nano Al disks. The black dash line is in agreement with the B1 region due to the PSPs propagating at the interface of Ag and Al_2O_3 layer whose resonance wavelength is determined by the following equations [22]:

$$k = k_0 \cdot \sin(\theta) \pm i \cdot \frac{2 \cdot \pi}{L} \tag{1}$$

$$k_{\mathrm{psp}} = k_0 \cdot \sqrt{\frac{\varepsilon_m \cdot \varepsilon_d}{\varepsilon_m + \varepsilon_d}} \tag{2}$$

Equation (1) is the Bragg coupling condition, in which $k_0 = \frac{w}{c}$ is the free-space wavevector, θ is the angle of the incident wave, i is the order of grating, L is the grating period. Equation (2) indicates the wavevector of the PSPs, ε_m and ε_d are the dielectric constant of metal (Al) and surrounding medium (Al_2O_3), respectively. Only when $k = k_{psp}$ does incident light couple to PSPs [23].

In contrast to Fig. 2a, absorption as a function of wavelength and radius r with fixing h = 36 nm, d = 24 nm, and L = 400 nm is shown in Fig. 2b. It is clear that the PSPs

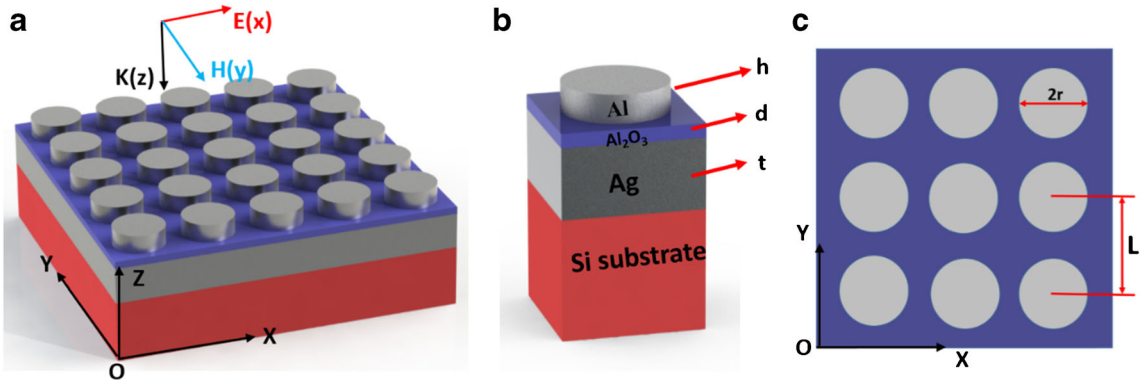

Fig. 1 **a** Schematic of the incident light polarization configuration and the super absorber which consists of Si substrate, a continuous Ag film, an Al_2O_3 spacing layer, and a nano Al disk array. **b** A unit of the super absorber with the thicknesses of Ag film, Al_2O_3 spacing layer, and Al disks are t = 100 nm, d, and h. **c** Top view of the absorber. The radius and period of nano Al disks are r and L

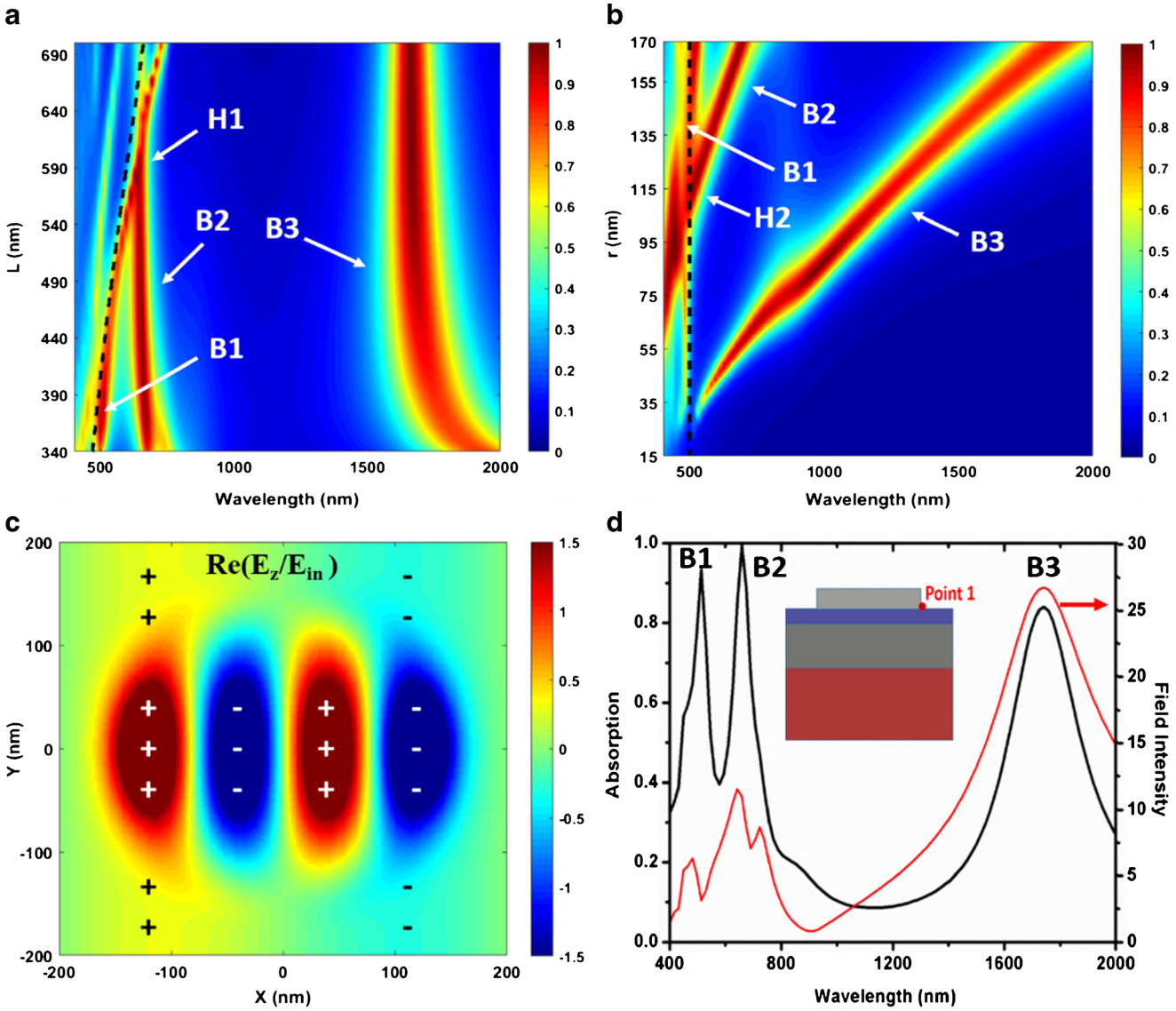

Fig. 2 **a** Absorption as a function of wavelength and the unit period L with fixing h = 36 nm, d = 24 nm, and r = 160 nm. **b** Absorption as a function of wavelength and radius r with fixing h = 36 nm, d = 24 nm, and L = 400 nm. The *black dash lines* both in **a** and **b** represent the calculated positions of PSPs using equations (1) and (2) in theory. H1 and H2 are the crosspoints of B1 and B2. **c** Electric field E_z vector and charge distributions at the Ag/Al_2O_3 interface at the resonance wavelength of PSPs with fixing h = 36 nm, d = 24 nm, L = 400 nm, and r = 160 nm. **d** The *black* and *red curves* corresponding to the *left* and *right y axis* represent the absorption spectrum and the near-field intensity at position 1 for an isolated disk, respectively, when h = 36 nm, d = 24 nm, r = 160 nm, and L = 400 nm

absorption peak B1 slightly depending on the nano disk radius r is exactly consistent with the black dash line which is calculated by equations (1) and (2) in theory. The inverse symmetric E_z distribution pattern in Fig. 2c corresponding to a symmetric surface charge distribution further demonstrates the PSPs mode with the characteristic of PSPs. While the LSPs modes B2 and B3 strongly depending on the radius r can be tuned in a wide range of wavelength band by changing r. A little increase in r will lead to a redshift of the absorption spectrum. For a larger r, exclusive of one main absorption peak B3 associated with the fundamental LSPs mode at the long wavelength, there is another peak B2 corresponding to the high-order LSPs at shorter wavelength. Therefore, the higher order absorption peak can be also used for the design of this kind absorber at visible wavelengths, which avoids using much smaller nanostructures. For example, in Fig. 2d, the black line is the absorption spectrum for r = 160 nm extracted from Fig. 2b. The absoption peaks are marked as B1 (513.13 nm, 93.48 %), B2 (658.58 nm, 99.62 %), and B3 (1741.41 nm, 84.07 %). There is a higher order absorption peak at the wavelength of 658.58 nm except the fundamental peak B3 (1741.41 nm). Since the enhanced electric field of LSPs is mainly confined in an extremely small volume near the nano Al disk, we monitor the electric field intensity at the

edge of one isolate nano Al disk on the top of Al_2O_3 spacing layer (the red point 1 shown in Fig. 2d) to measure the intensity of LSPs. As we can see, the electric field intensity is enhanced up to 26 times at the wavelength of 1741 nm consistent with the corresponding absorption peak B3, while the related electric field intensity at the wavelengths of peaks B1

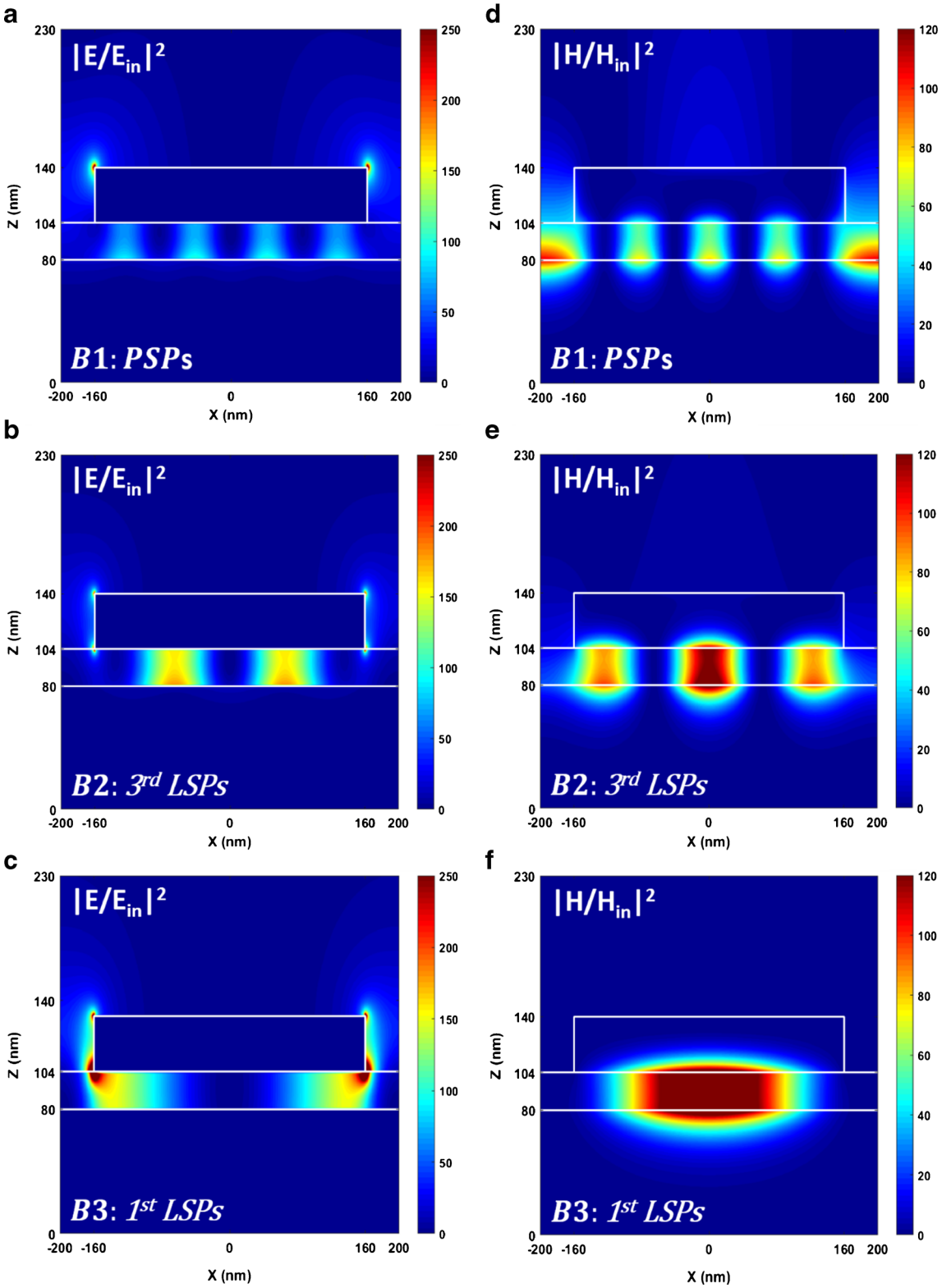

Fig. 3 The relative electric and magnetic field intensity distributions on the x-z plane of the three absorption peaks extracted from Fig. 2d for the absorber with L = 400 nm, r = 160 nm, h = 36 nm, and d = 24 nm

and B2 are very low, which proves that the electric field is not mainly confined at point 1 which we will discuss later.

To further verify the resonance conditions of the three absorption peaks in Fig. 2d, the relative electric and magnetic field distributions at three resonance wavelengths are simulated on the x-z plane. Figure 3a, d shows the relative electric and magnetic field distributions extracted from peak B1; the magnetic field intensity is mainly confined at the interface of the bottom Ag and the middle Al_2O_3 spacing layer, and the decay length into the metal is shorter than it in the dielectric medium, which indicate that the PSPs mode is excited by the incident wave coupled with the nano Al disk array. We have already attributed the absorption peak B3 to the excitation of fundamental LSPs, so that its electric field is strongly confined at the corners of the disk with a decay length of several decade nanometers shown in Fig. 3c, and the magnetic field is localized strongly in the Al_2O_3 spacing layer under the nano Al disk, which confirm the localized nature of the mode. For higher order LSPs B2, the electric field intensity distributions in Fig. 3b is weaker at the corners of the disk, but there is a strong E field enhancement in the spacing layer due to the high-order LSPs. It is evident from Fig. 3e that the oscillating magnetic field can form three antinodes, which is different from the just one antinode of the fundamental LSPs in Fig. 3f. It should be noted that one and three antinodes formed in the spacing layer indicate the excitation of first and third order LSPs, which is often called the "magnetic mode" [24].

To better understand the mechanism of ultrahigh absorption, the heat generation under light irradiation is investigated. It can be seen in Fig. 3 that the electromagnetic resonance modes supported by our MDM structure exhibit strong energy localization around the nano Al disks or in the Al_2O_3 spacing layer. The energy trapped by these resonance modes will be dissipated by the dielectric or Ohmic loss, which is to say, the incident light absorbed by the absorber is converted into dissipated heat ultimately. The Al_2O_3 layer is almost lossless within the wavelength we focus, so the energy only can be consumed in the metal Al and Ag by the means of Ohmic loss. In addition, the heat generated in the MDM absorber can be directly calculated numerically by using the local Ohmic loss for non-magnetic material [25]:

$$Q(r,w) = \frac{1}{2} \times w \times Im(\varepsilon) \times E^2(r,w) \tag{3}$$

In which w is the angular frequency, $Im(\varepsilon)$ is the imaginary part of the dielectric permittivity, and $E(r, w)$ is the local electric field. Here, the electric field intensity we used in the calculation is the relative values extracted from the FDTD simulation results in Fig. 3, so the heat $Q(r, w)$ calculated by equation (3) is not the true value but the relative distributions. Figure 4 shows the heat distributions for B1, B2, and B3 that represent the PSPs, 3rd LSPs, and 1st LSPs, respectively, when h = 36 nm, d = 24 nm, r = 160 nm, and L = 400 nm. The heat mainly generates in the bottom Ag layer in Fig. 4a due to the excitation of PSPs at the interface of Ag layer and Al_2O_3 spacing layer. While for LSPs, Fig. 4b, c, the heat generates both in the Ag layer and nano Al disks, which are consistent with the characters of the 3rd LSPs and 1st LSPs.

In the previous section, we have investigated the influence of single PSPs or LSPs on the absorption as well as the physical mechanism of the proposed absorber. Here, we will analyze the hybrid mode when the resonance wavelengths of PSPs and LSPs are the same. In many previous works [12, 24, 26], they usually focus on the hybrid mode due to the strong coupling between the PSPs and 1st order LSPs, which leads to an anticrossing behavior. While we found that in Fig. 2a, b, the resonance wavelengths of PSPs and LSPs can be tuned in a wide spectrum by changing the period L and the radius r. The absorption peaks B1 and B2 have crosspoints marked as H1 and H2 at which we can see the absorption can

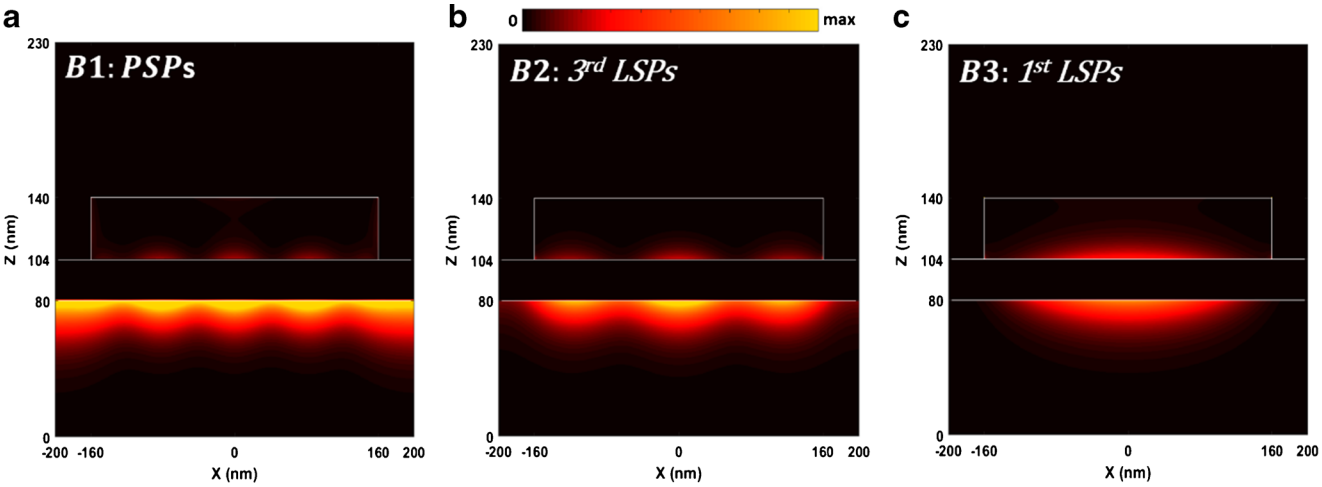

Fig. 4 Heat generation calculated by equation (3) when h = 36 nm, d = 24 nm, r = 160 nm, and L = 400 nm. **a**, **b**, **c** represent the peak B1, B2, and B3, respectively

be further enhanced. It is to say that our MDM structure can support both the PSPs and high-order LSPs at the same resonance wavelength. To prove this point, we choose period L = 600 nm and sweep r with fixing h = 36 nm, d = 24 nm. The simulation result is shown in Fig. 5b. Absorption peaks indicated by SP1 (Ag/Al_2O_3), 3rd LSPs, 1st LSPs have the same meaning as in Fig. 2b. SP0 (Al/Al_2O_3) is caused by the excitation of PSPs at the interface of nano Al disks and Al_2O_3 spacing layer, which is in agreement with the calculated result (dash white line) using equations (1) and (2). In the green box, an obvious anticrossing behavior is observed because of the strong coupling between the PSPs and 1st LSPs which is similar to the description in the references [12, 24, 26]. We extract r = 132, 164, and 188 nm (the three white lines) and give the absorption spectrums in Fig. 5a. As we can see, the peaks 3rd LSPs, SP1 are 61.76, 82.79 % at the wavelengths of 577.77, 642.42 nm, respectively, when r is 132 nm. Increasing r to the value of 164 nm, the two peaks SP1 and 3rd LSPs overlap with each other, forming one single absorption peak at the common resonance wavelength of 642.42 nm, which makes a contribution to an ultrahigh absorption 99.35 %. When the radius r is 188 nm, 3rd LSPs separates from SP1, and the absorption decrease to 86.61, 86.76 % at the wavelengths of 642.42, 723.23 nm, respectively. From the magnetic field distributions at the resonance wavelength 642.42 nm for r = 164 nm in Fig. 5c, the magnetic field is strongly confined both at the Ag/Al_2O_3 interface and in the Al_2O_3 spacing layer, which indicates that PSPs and 3rd LSPs modes are excited simultaneously at the same resonance wavelength. Hereto, we have demonstrated absorption can be further

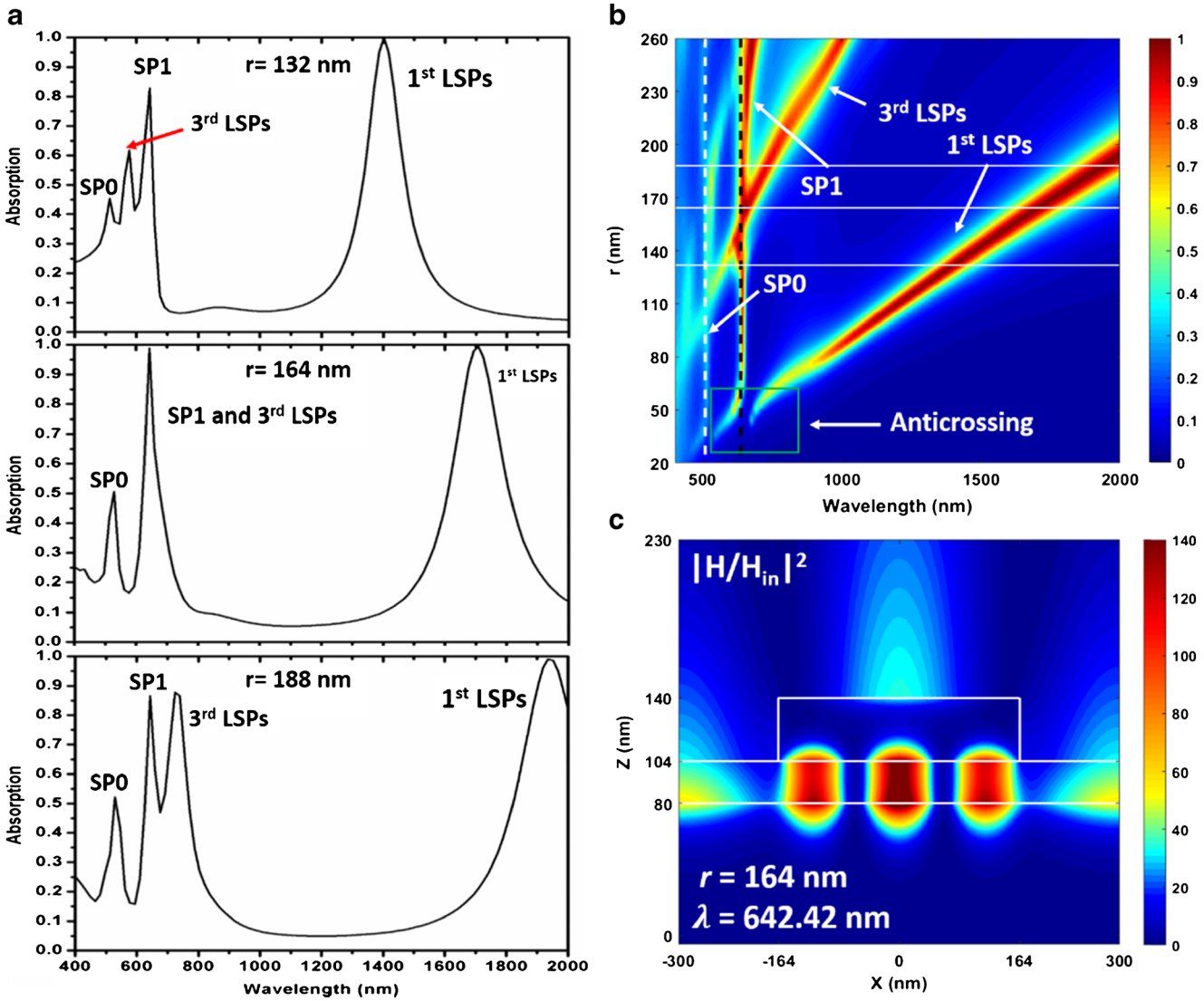

Fig. 5 Simulation results of the proposed absorber with L = 600 nm, h = 36 nm, d = 24 nm. **a** Absorption spectrums for r = 132 nm, 164 nm, and 188 nm. **b** Absorption as a function of wavelength and radius r. The *black* and *white dash lines* represent the calculated positions of PSPs using equations (1) and (2) in theory. The *three white lines* indicate three different r (132, 164, and 188 nm). **c** The magnetic field distributions at resonance wavelength of 642.42 nm for r = 164 nm

enhanced via tuning the resonance wavelengths of PSPs and high-order LSPs to be the same, which provides a new perspective in designing this kind of super absorber.

Conclusion

In conclusion, we have successfully proposed a super absorber based on PSPs and LSPs, which exhibits an ultrahigh (99.62 %) tunable absorption from visible to near-infrared spectrum by adjusting the period L and radius r. We thoroughly analyzed the PSPs and LSPs modes supported by the MDM structure and their relationship with the ultrahigh absorption. The mechanism of the absorber is also investigated which belongs to the consuming of the metal Ag and Al via Ohmic loss. And then, an obvious anticrossing behavior as a result of the strong coupling between the PSPs and 1st LSPs is observed. On this basis, a novel method to further enhance the absorption via the excitation of PSPs and high-order LSPs simultaneously is theoretically studied, which is different from previous works. Moreover, the use of stable Al instead of noble metal Au or Ag can be low cost and ease of processing, which makes this kind of novel absorber to be an appropriate candidate for photovoltaics, spectroscopy, sensing, photodetectors, and surface-enhanced Raman spectroscopy (SERS).

Acknowledgments Project supported by the National Natural Science Foundation of China (Nos. 61306125 and U1435210), the Science and Technology Innovation Project (Y3CX1SS143) of CIOMP, the Science and Technology Innovation Project of Jilin Province (Nos. Y3293UM130, 20130522147JH, and 20140101176JC), and the Science and Technology Innovation Foundation of CAS (CXJJ-15Q071).

References

1. Watts CM, Liu X, Padilla WJ (2012) Metamaterial electromagnetic wave absorbers. Adv Mater 24:98–120
2. Cheng S, Jie S, Wang X (2015) A design of thin film silicon solar cells based on silver nanoparticle arrays. Plasmonics 10:633–641
3. Yen-Hsun S, Ke Y-F, Cai S-L, Yao QY (2014) Surface plasmon resonance of layer-by-layer gold nanoparticles induced photoelectric current in environmentally-friendly plasmon-sensitized solar cell. Light Sci Appl 3:e222
4. Chalabi H, Schoen D, Brongersma ML (2014) Hot-electron photodetection with a plasmonic nanostripe antenna. Nano Lett 14:1374–1380
5. Park B, Yun SH, Cho CY, Kim YC, Shin JC, Jeon HG, Huh YH, Hwang I, Baik KY, Lee YI, Uhm HS, Cho GS, Choi EH (2012) Surface plasmon excitation in semitransparent inverted polymer photovoltaic devices and their applications as label-free optical sensors. Light Sci Appl 1:e14
6. Argyropoulos C, Le KQ, Mattiucci N, D'Aguanno G, Alu A (2013) Broadband absorbers and selective emitters based on plasmonic Brewster metasurfaces. Phys Rev B 87:205112
7. W. W. Salisbury, (June 10, 1952) Absorbent body for electromagnetic waves. U S patent 2:599-944.
8. Lee W, Kinosita Y, Youngjin O, Mikami N, Yang H, Miyata M, Nishizaka T, Kim D (2015) Three-dimensional super localization imaging of gliding Mycoplasma mobile by extraordinary light transmission through arrayed nano holes. ACS Nano 9:10896–10908
9. Hu XL, Sun LB, Beibei Z, Wang LS, Yu ZG, Bai SA, Yang SM, Zhao LX, Li Q, Qiu M, Tai RZ, Fecht HJ, Jiang JZ, Zhang DX (2016) Polarization-independent plasmonic subtractive color filtering in ultrathin Ag nanodisks with high transmission. Appl Opt 55(1):148–152
10. Chu Y, Banaee MG, Crozier KB (2010) Double-resonance plasmon substrates for surface-enhanced Raman scattering with enhancement at excitation and stokes frequencies. ACS Nano 4:2804–2810
11. Dayal G, Anantha Ramakrishna S (2012) Design of highly absorbing metamaterials for infrared frequencies. Opt Express 20(16): 17503–17508
12. Chen J, Hu J (2014) Strong coupling between localized and propagating surface plasmon modes in a noncentrosymmetric metallic photonic slab. J Opt Soc Am B 31(7):1600–1606
13. Wang BX, Zhai X, Wang GZ, Huang WQ, Wang LL (2015) A novel dual-band terahertz metamaterial absorber for a sensor application. J Appl Phys 117:014504–014501
14. Dong X, Tao K, Wang Q (2015) Ultrabroadband mid-infrared light absorption based on a multi-cavity plasmonic metamaterial Array. Plasmonics 10:1007
15. Lin C-H, Chern R-L, Lin H-Y (2011) Polarization-independent broad-band nearly perfect absorbers in the visible regime. Opt Express 19(2):415–424
16. Hao J, Wang J, Liu X, Padilla WJ, Zhou L, Qiu M (2010) High performance optical absorber based on a plasmonic metamaterial. Appl Phys Lett 96:251104
17. Li Y, An B, Jiang S, Gao J, Chen Y, Li SPY, An B, Jiang S, Gao J, Chen Y, Pan S (2015) Plasmonic induced triple-band absorber for sensor application. Opt Express 23(13):17607–17612
18. Knight MW, King NS, Liu L, Everitt HO, Nordlander P, Halas NJ (2014) Aluminum for plasmonics. ACS Nano 8:834–840
19. Knight MW, Liu L, Wang Y, Brown L, Mukherjee S, King NS, Everitt HO, Nordlander P, Halas NJ (2012) Aluminum plasmonic nanoantennas. Nano Lett 12:6000–6004
20. Palik ED (1998) Handbook of optical constants of solids. Academic, New York
21. Zheng YB, Juluri BK, Mao X, Walker TR, Huang TJ (2008) Systematic investigation of localized surface plasmon resonance of long-range ordered Au nanodisk arrays. J Appl Phys 103:014308
22. Li G, Yang S, Xiao G, Jin C (2015) Double-layered metal grating for high performance refractive index sensing. Opt Express 23(7): 8995–9003
23. Genet C, Ebbesen TW (2007) Light in tiny holes. Nature 445:39–46
24. Chen J, Wang P, Zhang ZM, Lu Y, Ming H (2011) Coupling between gap plasmon polariton and magnetic polariton in a metallic-dielectric multilayer structure. Phys Rev E 84:026603
25. Li W, Valentine J (2014) Metamaterial perfect absorber based hot electron photodetection. Nano Lett 14:3510–3514
26. Chu Y, Crozier KB (2009) Experimental study of the interaction between localized and propagating surface plasmons. Opt Lett 34(3):244–246